



RESEARCH ARTICLE

10.1002/2015WR018364

Key Points:

- Interflow thresholds ranged from 131 to 208 mm, and flow paths were state-dependent
- Event-water fractions increased nearly linearly as irrigation progressed, reaching a maximum of 50% after 407 mm of irrigation
- Hillslope fluxes integrate spatiotemporal-varying processes controlled by conductivity, soil depth, and subsurface detention distributions

Correspondence to:

C. R. Jackson,
rjackson@warnell.uga.edu

Citation:

Jackson, C. R., E. Du, J. Klaus, N. A. Griffiths, M. Bitew, and J. J. McDonnell (2016), Interactions among hydraulic conductivity distributions, subsurface topography, and transport thresholds revealed by a multitracer hillslope irrigation experiment, *Water Resour. Res.*, 52, 6186–6206, doi:10.1002/2015WR018364.

Received 11 NOV 2015

Accepted 19 JUL 2016

Accepted article online 22 JUL 2016

Published online 12 AUG 2016

Interactions among hydraulic conductivity distributions, subsurface topography, and transport thresholds revealed by a multitracer hillslope irrigation experiment

C. R. Jackson¹, Enhao Du¹, Julian Klaus², Natalie A. Griffiths³, Menberu Bitew¹, and Jeffrey J. McDonnell^{4,5}

¹Warnell School of Forest Resources, University of Georgia, Athens, Georgia, USA, ²Environmental Research and Innovation Department, Luxembourg Institute of Science and Technology, Esch-sur-Alzette, Luxembourg, ³Climate Change Science Institute and Environmental Sciences Division, Oak Ridge National Laboratory, Oak Ridge, Tennessee, USA, ⁴School of Environment and Sustainability, University of Saskatchewan, Saskatoon, Saskatchewan, Canada, ⁵School of Geosciences, University of Aberdeen, Scotland, UK

Abstract Interactions among hydraulic conductivity distributions, subsurface topography, and lateral flow are poorly understood. We applied 407 mm of water and a suite of tracers over 51 h to a 12 by 16.5 m forested hillslope segment to determine interflow thresholds, preferential pathway pore velocities, large-scale conductivities, the time series of event water fractions, and the fate of dissolved nutrients. The 12% hillslope featured loamy sand A and E horizons overlying a sandy clay loam Bt at 1.25 m average depth. Interflow measured from two drains within an interception trench commenced after 131 and 208 mm of irrigation. Cumulative interflow equaled 49% of applied water. Conservative tracer differences between the collection drains indicated differences in flow paths and storages within the plot. Event water fractions rose steadily throughout irrigation, peaking at 50% sixteen h after irrigation ceased. Data implied that tightly held water exchanged with event water throughout the experiment and a substantial portion of pre-event water was released from the argillic layer. Surface-applied dye tracers bypassed the matrix, with peak concentrations measured shortly after flow commencement, indicating preferential network conductivities of 864–2240 mm/h, yet no macropore flow was observed. Near steady-state flow conditions indicated average conductivities of 460 mm/h and 2.5 mm/h for topsoils and the Bt horizon, respectively. Low ammonium and phosphorus concentrations in the interflow suggested rapid uptake or sorption, while higher nitrate concentrations suggested more conservative transport. These results reveal how hydraulic conductivity variation and subsurface topographic complexity explain otherwise paradoxical solute and flow behaviors.

1. Introduction

The Darcy velocity and the representative elemental volume concept have been effective concepts for simplifying complex flow fields into tractable problems amenable to Richards or Darcy analysis. The utility of these simplifications tends to obscure the fact that any hillslope or watershed features a distribution of hydraulic conductivities [Kung *et al.*, 2005], interflow generation thresholds [Uchida *et al.*, 2005], and networks of individual water flow paths [Graham and McDonnell, 2010]. Irrigation experiments can provide a window into these hillslope flow complexities. Hillslope irrigation experiments can reduce the noise that may confound inference from hydrologic observations during natural events. They also allow more precise, large-scale estimates of hillslope hydraulic characteristics, the magnitude of internal storages, and flow generation thresholds.

Irrigation experiments have been conducted since the 1960s [Hewlett and Hibbert, 1963] with tracer-based approaches popularized in the early 1990s [Hornberger *et al.*, 1991]. More recent irrigation work has focused on hillslope water balances [Tromp-van Meerveld *et al.*, 2007; Graham *et al.*, 2010a, 2010b], estimates of plot-to-hillslope scale conductivity [Brooks *et al.*, 2004; Tromp-van Meerveld *et al.*, 2007], characterization of bypass flow through preferential pathways [Kung *et al.*, 2000; Steenhuis *et al.*, 1994], estimates of preferential network conductivities [Weiler and McDonnell, 2007; Anderson *et al.*, 2009; Klaus *et al.*, 2013], characterization of piezometric behavior across the plot [Bachmair and Weiler, 2014], examination of solution chemistry

dynamics and mixing [Garel *et al.*, 2012; Klaus *et al.*, 2013], and illumination of process dynamics at the hillslope scale [e.g., McGuire *et al.*, 2007; Graham *et al.*, 2010b; Garel *et al.*, 2012; Debieche *et al.*, 2012]. When evaluated in isolation, individual tracers can produce different and even contradictory inferences about hydrologic processes (see the progression of research at Maimai catchments in New Zealand, summarized by McGlynn *et al.* [2002]). When evaluated together with hydrometric information, multiple tracers can reveal a more complete and holistic understanding of flow processes.

Past work has added to our understanding of the individual pieces of hillslope systems, but more experiments are needed to fuse these pieces together and to understand the threshold release of water (so common in natural rainfall events) of mixed age and flowpath. Here we simultaneously examine Darcy velocities, pore velocities, thresholds, and state variables to examine the ensemble behavior of hillslope flow paths and resulting fluxes. We applied controlled irrigation and a suite of conservative and nonconservative tracers to illuminate how distributions of conductivities and state-dependent flow paths affect water and tracer fluxes at the hillslope scale. The 12 m \times 16.5 m forested hillslope segment used for our irrigation experiment is a simple planar 12% slope with little surface microtopography and loamy sand A and E horizons (hereafter referred to jointly as topsoils) overlying a sandy clay loam Bt horizon at an average depth of about 1.25 m. Previous observations of the larger hillslope found that perching above the Bt horizon was common, but interflow was not [Du *et al.*, 2016]. Furthermore, interflow was largely disconnected from streamflow behavior. Interflow was highly variable across 11 segments of a 120 m trench, and macropore flow was not observed at the trench face. Three-dimensional Richards Equation modeling with HYDRUS 3D suggested a large interflow generation threshold (approximately 160 mm of preevent soil water and event water, or 80 mm of event water, (L. Hopp, personal communication, 2015), and field observations over several years [Du *et al.*, 2016] indicated a slightly lower event threshold of 60 mm (events occurred when soils were wet). These interflow generation threshold estimates lie at the highest end of the range of such thresholds [Uchida *et al.*, 2005; Ali *et al.*, 2015]. Part of the motivation for applying controlled irrigation to this slope was to test these estimates of interflow generation thresholds. We were also motivated to measure topsoil and Bt layer conductivities to estimate likely downslope travel distances [Jackson *et al.*, 2014] and thereby determine whether short travel distances are an explanation for observed hillslope-stream disconnection observed in this and adjacent catchments [Klaus *et al.*, 2015; Du *et al.*, 2016; Griffiths *et al.*, 2016].

With this experiment, we tackle the following specific questions: 1) What is the rainfall plus antecedent soil moisture threshold necessary to initiate interflow?, 2) Is interflow over an argillic Bt horizon consistent with the fill and spill concept?, 3) How does the preevent/event water ratio vary through a large event?, 4) What are the plot scale average conductivities of the restrictive Bt horizon and the overlying A and E horizons?, 5) How do these average conductivities compare to conductivities determined from dye tracer velocities?, 6) Is interflow behavior on this slope consistent with simple estimates of downslope travel distances?, and 7) What is the fate of dissolved nitrogen and phosphorus in rainwater as it moves through the soil?

Most studies examining the relative contribution of event (new) and preevent (old) water to stormflow generation have looked at stream water chemistry relative to the chemistry of hillslope and throughfall end members [e.g., Pearce *et al.*, 1986; Sklash *et al.*, 1986; Mulholland, 1993]. These event/preevent fraction determinations are often hampered by temporal variation in the chemistry of the identified hillslope pools [Buttle and Peters, 1997] and the lack of solutes or isotopes that clearly differentiate these pools [e.g., Soulsby *et al.*, 2003; Carrera *et al.*, 2004]. Within hillslopes and watersheds, event/preevent water fractions and end-member fractions vary substantially within and among storms [e.g., Ali *et al.*, 2010; Harpold *et al.*, 2010; Garrett *et al.*, 2012; Klaus and McDonnell, 2013]. Explaining such variation is difficult when each natural storm has different initial conditions, timing, and total depth. These variables may alter estimates of end member contributions by 30% [Delsman *et al.*, 2013]. By introducing bromide (Br⁻) (which has a negligible background concentration) to the feedwater, we create an unambiguous signature for event water in interflow draining the hillslope. This experiment also allowed us to characterize the time series of event water fraction relative to storm size.

Previous work on this hillslope suggested discrepancies between topsoil conductivities estimated from trench flow rates and those measured with a compact constant head permeameter [Du *et al.*, 2016]. Brooks *et al.* [2004] found that large-scale estimates of surface soil conductivities were up to 13.7 times larger than the median values of small-scale measurements. They inferred that macroporosity, possibly of biological origin, was often missed by small-scale measurements. Previous small-scale compact constant head

permeameter measurements of Bt horizon conductivities within our watershed [Du *et al.*, 2016] and in the nearby Panola watershed [Appels *et al.*, 2015] found large variability of several orders of magnitude. This experiment was partly motivated by our need for large-scale conductivity estimates to parameterize watershed models and to understand dominant hydrologic pathways.

Macropore flow has never been observed at this trench face [Du *et al.*, 2016], but it is expected that the soil matrix features preferential flow pathways. We applied dye tracers to the ground surface on transects two different distances from the trench to estimate tracer velocities and conductivities associated with the fastest flow paths and to evaluate maximum downslope travel distances [Jackson *et al.*, 2014]. When tracers are applied on the ground prior to irrigation and allowed to dissolve with the incoming precipitation, the highest concentrations occur with the earliest-arriving water because the source is depleted as the event continues [e.g., McDonnell *et al.*, 1998; McGuire *et al.*, 2007]. Thus the tracer breakthrough characterizes transport through the preferential flow network [Anderson *et al.*, 2009]. Surface-applied dye tracers also allow estimation of potential contributing distances from upslope [e.g., McGuire and McDonnell, 2010]. It can be difficult to interpret pore velocities when surface tracers are mobilized by natural rainfall events too small to mobilize all of the tracer [e.g., Tromp-van Meerveld *et al.*, 2007]. With a large depth of irrigation, a clear estimate of the pore velocities associated with peak tracer concentrations is possible.

Nutrients (N and P) were applied to examine the time series of nutrient outflows and thereby develop inference about nutrient uptake, transformations, and sorption processes. Nutrients (primarily N) can enter forested ecosystems via atmospheric deposition [Lindberg *et al.*, 1986; Driscoll *et al.*, 2003]. In areas where N or P limits forest productivity, nutrients are recycled with little export. However, when forest uptake rates are low (i.e., in winter), excess nutrients can enter adjacent water bodies [Barnes *et al.*, 2008; Sebestyen *et al.*, 2008] and can cause water quality issues such as eutrophication [Howarth *et al.*, 1996; Vitousek *et al.*, 1997]. Nitrate is the nutrient of most concern as it tends to travel more conservatively than ammonium and phosphate due to its negative charge. This hillslope irrigation experiment provides an opportunity to examine the combined fate (assimilatory and dissimilatory uptake, mixing, and sorption processes) of nutrients (nitrate, ammonium, phosphorus) in precipitation on a forested hillslope and the coupled dynamics between hydrological and nutrient cycles.

2. Methods

2.1. Site Description

The study hillslope segment is a 12% planar slope with little surface microtopography, supporting a 42 year-old planted loblolly pine stand with scattered hardwoods. The hillslope drains to an intermittent tributary of Fourmile Creek (watershed R as described in Klaus *et al.* [2015]; Du *et al.* [2016]; Griffiths *et al.* [2016]) in the Sandhills physiographic province comprising the geologic interface between the Piedmont and Upper Coastal Plain of the southeastern United States. Prior to pine planting, the slope had been in row-crop farming for many decades before the United States government created the Savannah River Site (SRS) for the production and management of tritium. The SRS is located to the southeast of Aiken, South Carolina, USA, and is now a National Environmental Research Park. Soils are Ultisols of the Fuquay sand series formed on marine terraces. Soils feature a thin A horizon and a deep E horizon, both composed of loamy sands with low organic matter content and high bulk densities (1.6 to nearly 1.9 g cm⁻³). The A and E horizons overlie a transitional BE horizon of varying thickness over an argillic sandy clay loam Bt horizon of similar bulk density to the topsoils. Augering and trenching reveal that the argillic Bt horizon features layers of varying bulk density and firmness. The surface of the Bt horizon is irregular, with a high density of concavities. Depths to the Bt horizon measured on a 2 x 4 m grid within the plot area ranged from 0.95 to 1.53 m and averaged 1.25 m with a standard deviation of 0.18 m. Based on previous argillic depth measurements at 0.25 m spacing along the trench face [Du *et al.*, 2016], we know that Bt topography is more irregular than indicated by the 2 x 4 m grid, and the grid resolution is not sufficient to map the subsurface depressions and drainage patterns. Argillic layer thickness averages about 2 m, and more loamy sands are found below the argillic layer [Du *et al.*, 2016]. Infiltration rates are high, and Hortonian overland flow is not observed. Mean annual temperature is 18°C, and average monthly temperatures range from 1.4°C in January to 33.6°C in July. Average annual precipitation is 1225 mm distributed fairly evenly through the year [Kilgo and Blake, 2005].

Table 1. Weather Observations Prior to and During the Irrigation Experiment as Obtained From SRS Central Meteorological Tower and Tipping Bucket^a

Data Type	Observation Period						
	March 2012	1–9 Apr	9 Apr	10 Apr	11 Apr	12 Apr	
Daily temperature, °C	MAX	26.5	31.9	32.3	33.1	26.7	27.0
	Mean	17.6	19.0	18.3	19.2	15.6	12.4
	MIN	10.9	11.7	9.6	7.2	5.1	2.7
Average daily wind speed, m/s	1.90	1.68	1.26	2.62	2.62	1.67	
Average daily solar radiation, Wh/m ²	4357.3	6083.8	7218.4	7147.4	7414.8	7474.0	
Daily Pan evaporation depth, mm	0.73	0.91	0.56	unknown	0.73	0.42	
Sun Hour, hr	15	13	13	13	13	14	
Total precipitation, mm	77.74	31.00	0	0	0	0	
		(4/5)					
		0.25					
Soil Moisture, m ³ /m ³	Shallow	0.0520	0.0548	0.0516	0.0481	0.0448	0.0424
	Deep	0.1339	0.1429	0.1369	0.1305	0.1253	0.1212
Total PET from PM, mm	97.26	38.97	5.03	6.21	5.36	4.37	

^aPotential Evapotranspiration (PET) calculated with Penman-Monteith (PM) equation for grass without water limitation.

2.2. Climate Conditions Prior To and During the Experiment

Rainfall for the month preceding the experiment (the month of March 2012) was 25% below normal. A 31 mm rainfall occurred on 5 April, 5 days before the experiment commenced. Overall, climate and soil moisture conditions were typical for the season (see weather summary, Table 1). No natural rainfall fell during the irrigation experiment.

2.3. Plot Size and Monitoring System

The irrigated area, determined by visual inspection during irrigation, was 12 × 16.5 m (198 m²) and was fed by 24 regularly spaced irrigation sprinklers with replaceable heads to control irrigation rates (see orientation in Figure 1). The lower extent of irrigation application was about 0.75 m upslope of the trench face. The plot area and perimeter contained one nest of recording piezometers (one at the argillic layer interface, one within the argillic layer, and one below the argillic layer), sixteen hand-checked piezometers installed 8–10 cm into the argillic layer, and three sets of recording soil moisture sensors. The sixteen hand-checked piezometers were installed (eleven within the irrigation area and five just outside the perimeter of the irrigation area, all in four rows, Figure 1) to monitor the formation and progression of the perched water table and to access samples of perched water. One set of soil moisture sensors was located at the base of the plot, another set was arrayed across the plot below piezometer row 2, and the final set was arrayed near the top of the plot between piezometer row 3 and 4. Each set of soil moisture sensors consisted of 5 cm TDR probes, installed vertically, with shallow probes

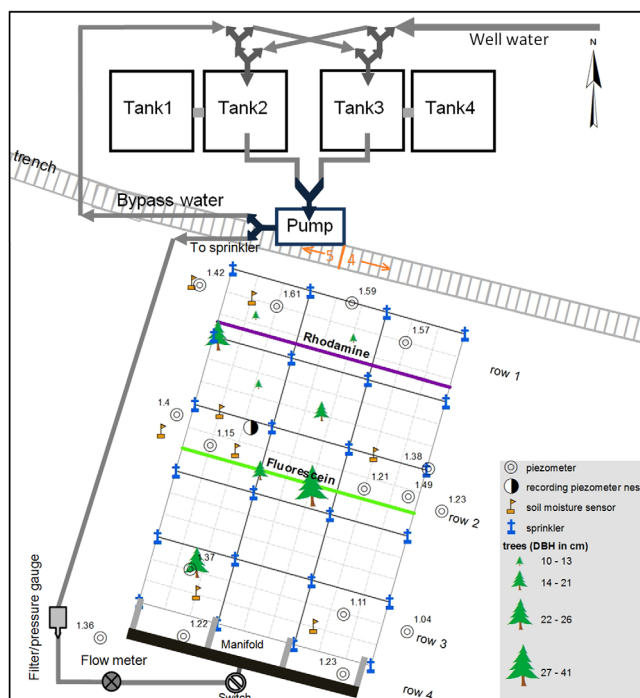


Figure 1. Irrigated plot schematic. Irrigated area did not extend all the way down to the trench with about 0.75 m not irrigated between the trench and the plot (see Figure 5). Two separately piped sections (4 and 5) of the 120 m long trench lie below the irrigation area. Numbers next to piezometers indicate piezometer depth (m). Plot area is drawn to scale (each grid square is 1 m × 1 m), but irrigation system is not.

inserted from the ground surface in the topsoil, and deeper probes inserted into the BE transition horizon, usually at 80–100 cm depth. Eight pine trees of various sizes (Figure 1) grew within the plot, which itself was located within a mature planted pine stand.

2.4. Irrigation Rates and Timing

Our goal was to initiate interflow and then achieve near steady-state conditions at an application rate 1.5–2 times greater than the previously measured average conductivity of the Bt horizon (3 mm/h). However, because we also expected an interflow initiation threshold in the range of 60–160 mm, we were concerned about the duration of the experiment necessary to create interflow and reach steady-state conditions. Therefore, irrigation was conducted in two phases, with a higher initial rate designed to initiate perching above the argillic horizon and interflow at the trench (Phase I), followed by a reduced application rate (Phase II) designed to achieve steady-state interflow and percolation without saturating the profile.

2.4.1. Phase I

We initially applied irrigation water at approximately 14 mm/h, but the rate dropped in the first night to about 11 mm/h, apparently due to clogging and ineffective cleaning of the filter. This phase I application rate was maintained until perching occurred in the row 1 piezometers and flow initiated at the trench. Phase I was terminated at 18:48 h after applying 213 mm of water, about half of the total applied water. Throughout this paper, clock times will be noted with am or pm, and otherwise times will be reported as time (hours:mins) since initiation of irrigation.

2.4.2. Phase II

After Phase I was completed, we turned off the pumps for approximately 10 min to change the sprinkler heads. In Phase II, irrigation rates were very constant at 6 mm/h, and this rate was sustained for 32:20, over which time 194 mm of water was applied to the plot. We terminated irrigation when a reasonable approximation of steady-state hydrometric conditions had been achieved as determined by low rates of change in piezometer depth behavior and trench outflows. We had intended to also use near-constant specific conductivity levels of the outflow water as a marker of steady-state conditions, but event/preevent water fractions changed continuously and never approached a steady-state of solute flux (see Results).

Irrigation began at 2:45 pm on 10 April 2012, and continued for 51 h 18 min, ending at 6:03 pm on 12 April 2012. Water from a deep irrigation well (screened interval 142–152 m) was pumped into four nominal 9460 L capacity folding tanks into which bromide and nutrients were added. The four feedwater tanks were set up as two connected pairs each filled and mixed with bromide and nutrients prior to application. Water was pumped from one pair of tanks to 24 Eindoor sprinkler heads placed on a 2 × 4 m grid within the plot (Figure 1). A cumulative flow gage (NETAFIM M series 1" (25.4 mm) iron water meter) on the feed line measured the amount of water applied. The effective capacity of each tank was back-calculated as 6720 L, based on the total applied volume. In total 80,605 L of water or 407 mm were applied to the plot. This artificial event was equivalent to one third of average annual precipitation for this humid temperate forest falling in a little more than 2 days. The final choice of applied volume was based on reaching a near steady-state hydrologic condition, and we did not design the artificial event to correspond to any particular return interval. Coincidentally, much of South Carolina experienced greater precipitation over a similar length of time during the Hurricane Joaquin event of 1–5 October 2015 [Feaster *et al.*, 2015].

2.5. Tracer Additions

2.5.1. Fluorescent Dyes

Rhodamine WT dye tracer was applied on contour 4.5 m above the trench, and Fluorescein green was applied on contour 10 m from the trench. Each dye tracer was applied with a backpack sprayer on a line transect across the width of the plot at the start of the experiment (Figure 1). A solution of 150 mL of concentrated Rhodamine WT mixed into 5 L of water was applied along the lower line transect (near row 1 piezometers) after removing the leaf litter and vegetation from the ground surface. A fluorescein solution of 50 mL of concentrated Fluorescein green mixed into 5 L of water was equivalently applied along the middle line transect (near row 2 piezometers). Rhodamine is moderately resistant (Soil adsorption coefficient [K_{oc}] = 1700–20,000 cm³ g⁻¹) and fluorescein is highly resistant (K_{oc} = 120 cm³ g⁻¹) to soil sorption [Shiau *et al.*, 1993; Kasnavia and Sabatini, 1999], but fluorescein is subject to photodegradation. The dyes were applied at 1:00 pm on 10 April 2012 just prior to commencing irrigation at 2:45 pm, and the fluorescein was protected from the sun by covering the dye application transect with pine straw native to the site. The sun

set at 7:54 pm, and no dye was visible at the surface the next morning. We therefore considered photodegradation negligible.

2.5.2. Conservative Tracers—Bromide and Feedwater Isotope Signature

All irrigation water was labeled with an approximately constant concentration of bromide. 141 g of KBr were mixed in every tank (average realized capacity of 6720 L), yielding a target solution of 14 mg/L. However, measured feed water concentrations averaged 12.9 mg/L, apparently due to incomplete mixing. Electric trolling motors and wooden canoe paddles were used to stir the water in the tanks. Irrigation water was drawn from a deep semiconfined aquifer with a $\delta^{18}\text{O}$ value of -22.6‰ and a $\delta^2\text{H}$ of -4.1‰ . This signal is different from the average observed stable isotope composition in rainfall on site ($\delta^{18}\text{O} = -3.1\text{‰}$ and $\delta^2\text{H} = -13.8\text{‰}$) and from soil water that is likely that enriched in heavy isotopes compared to precipitation (as shown by Klaus *et al.* [2015]), supplying an identifiable isotopic end member.

2.5.3. Nitrogen and Phosphorus

Nitrogen (as nitrate and ammonium) and phosphorus (as phosphate) were added to the irrigation water in order to examine the fate of nutrients on the hillslope. The target nutrient concentrations in the irrigation water were 1 mg N/L for both ammonium and nitrate, and 40 μg P/L for phosphate. These concentrations were selected as they are similar (but on the high end) to the nutrient content of throughfall measured in the study watershed and thus represent nutrient inputs during a rainfall event [Griffiths *et al.*, 2016; N. A. Griffiths, unpublished data (for P)], 2015.

Nutrient stock solutions were made by dissolving 108 g of ammonium nitrate (NH_4NO_3) and 3.3 g of monopotassium phosphate (KH_2PO_4) in 1 L of deionized water. One stock solution (1 L) was then added to each set of tanks, and mixed with a paddle before applying to the hillslope. The mean measured concentrations of added nutrients in the tanks were 902 μg N/L nitrate, 1236 μg N/L ammonium, and 33 μg P/L soluble reactive phosphorus. The total mass of nutrients applied to the hillslope over the experiment was 72.7 g N of nitrate, 99.6 g N of ammonium, and 2.7 g P of phosphate, respectively.

2.6. Trench Outflows and Water Budget

The irrigated plot drained to two of 11 sections of a 120 m long open interflow interception trench cut on contour about 0.7 m into the Bt horizon [Du *et al.*, 2016]. Each section was underlain by a French drain consisting of a perforated pipe beneath 0.45 m of gravel. Approximately 7 m of the plot width was situated above section 4 of the trench, and the remaining 5 m of the plot was above section 5 (Figure 1). Water collected in each French drain was piped downslope to 30 degree V-notch weir boxes (flumes 4 and 5) instrumented with recording capacitance probes that measured stage every 10 min. Both flumes included a staff gage that was periodically monitored to check the automatically recorded stages and corrections were applied if necessary. The trench face was regularly inspected during the experiment for water staining, seepage, and the occurrence of observable macropore flow.

Pre- and postexperiment soil water storage was estimated by averaging all soil moisture TDR probe readings in the top soil (1.25 m thick) and the first meter of the argillic clay (compared to the total argillic layer thickness of 2 m) assuming that only the upper half of the layer was involved in the storage change. Any storage change below this level went into the residual of percolation and unaccounted water. The initial soil water contents for the topsoil and argillic layer were 0.10 and 0.18 vol vol⁻¹, or 125 and 180 mm, respectively.

We used the Penman-Monteith equation [Monteith, 1965] to estimate grass reference (ET_0) over the experiment based on the procedures outlined in Allen *et al.* [2000]. We used hourly solar radiation ($\text{W m}^{-2} \text{d}^{-1}$), air temperature ($^\circ\text{C}$), wind speed (m s^{-1}), and humidity aggregated from 15 min high resolution climate data from the SRS Central Climate Tower located 5 km from the irrigation plot.

2.7. Sampling

The maximum rise piezometers and the trench outflow were checked once an hour in daylight hours, and once every 2 h in evening hours until perching and outflow occurred. Once perching or flow was observed, regular sampling began. Water samples were collected from the flumes and hillslope piezometers during the experiment to determine conservative tracer (Br⁻), fluorescent dye (rhodamine WT, fluorescein), and nutrient (nitrate, ammonium, and soluble reactive phosphorus) concentrations and the stable isotopes of water and nitrate ($\delta^2\text{H}_{\text{H}_2\text{O}}$, $\delta^{18}\text{O}_{\text{H}_2\text{O}}$, $\delta^{15}\text{N}_{\text{NO}_3}$, $\delta^{18}\text{O}_{\text{NO}_3}$). Water samples were collected from the tanks each time they were filled to determine initial nutrient, bromide, and isotope concentrations. Composite samples

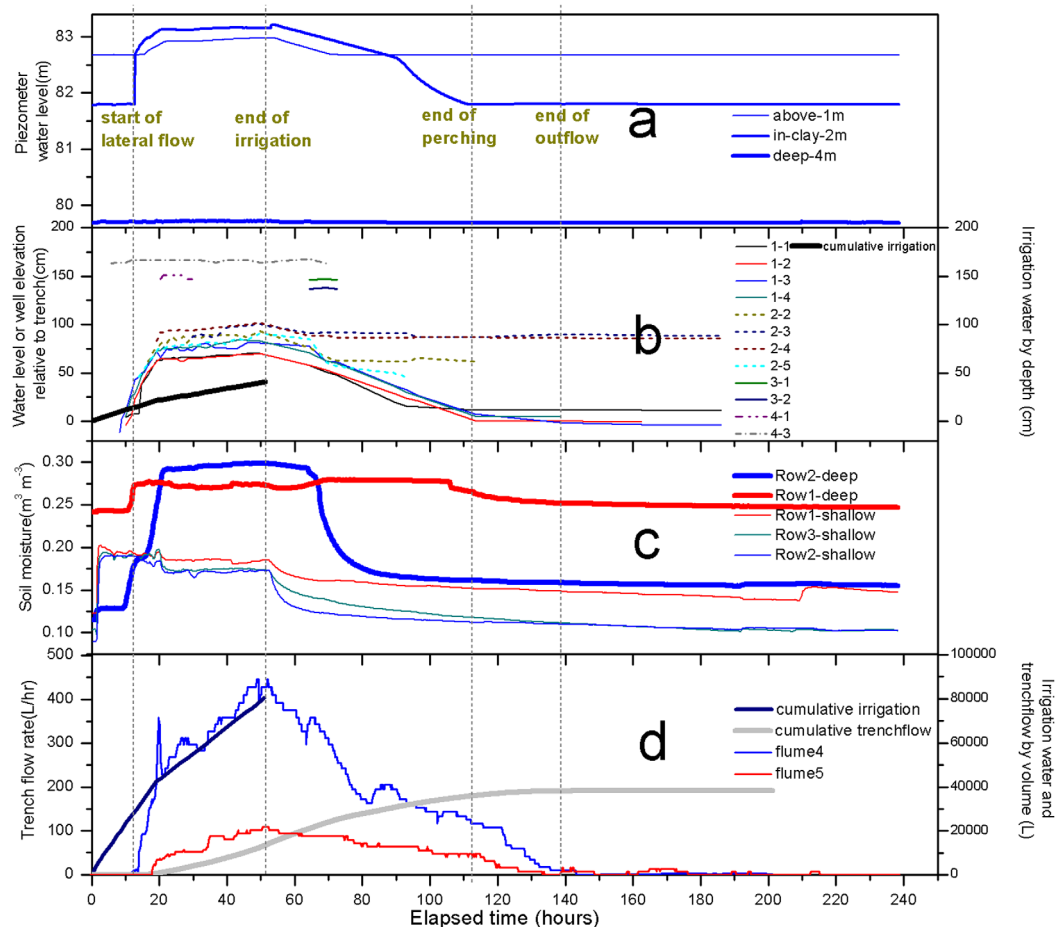


Figure 2. Time series of (a) water levels in recording piezometers, (b) water levels in hand measured piezometers, (c) soil moisture percentages, and (d) instantaneous and cumulative trench outflows over the course of the experiment. Irrigation rate is reduced at 19 h (see break in cumulative irrigation line in Figure 2d).

from all the hand-checked piezometers were taken approximately every 3 h during the experiment, and the flumes were sampled every 1–2 h. When both flumes 4 and 5 were flowing, a flow-weighted composited sample was collected from both flumes and analyzed for chemistry. Samples for bromide analysis were collected from each flume over much of the experiment because specific conductivity measurements indicated differences in the chemistry of the two flumes and we wanted to examine spatial heterogeneity in hillslope hydrologic processes including if event/preevent water fractions varied between the flumes. Measurements of trench flow, piezometer water level, soil moisture, and sampling for tracers occurred during Phase I and Phase II, and then for 150–190 h during the recession period (after the irrigation was turned off) (Figure 2). Occasional bromide and isotope samples were taken from the trench outflow for 65 h following cessation of irrigation (Figure 3).

2.8. Chemical, Dye, and Isotope Analyses

All nutrient samples were filtered in the field (GF/F, 0.7 μm nominal pore size) into acid-washed, HDPE bottles. Samples were kept on ice and then frozen at -20°C in the laboratory until analysis. Nitrate-N concentrations were measured using the cadmium reduction method, ammonium-N concentrations with the phenol-hypochlorite method, and soluble reactive phosphorus (SRP) concentrations with the molybdate-antimony method [APHA, 2005] on a SEAL AutoAnalyzer 3 (SEAL Analytical). Analysis of water samples for stable isotopes of nitrate ($\delta^{15}\text{N}_{\text{NO}_3}$ and $\delta^{18}\text{O}_{\text{NO}_3}$) was done at the UC Davis Stable Isotope Facility using the denitrifier method with *Pseudomonas aureofaciens* bacteria [Sigman et al., 2001; Casciotti et al., 2002].

The bromide tracer was analyzed with a Dionex ICS-1500 Ion Chromatograph combined with a Dionex AS40 Automated Sampler. The detection limit for bromide was 0.01 mg/L with a precision of 0.01 mg/L for

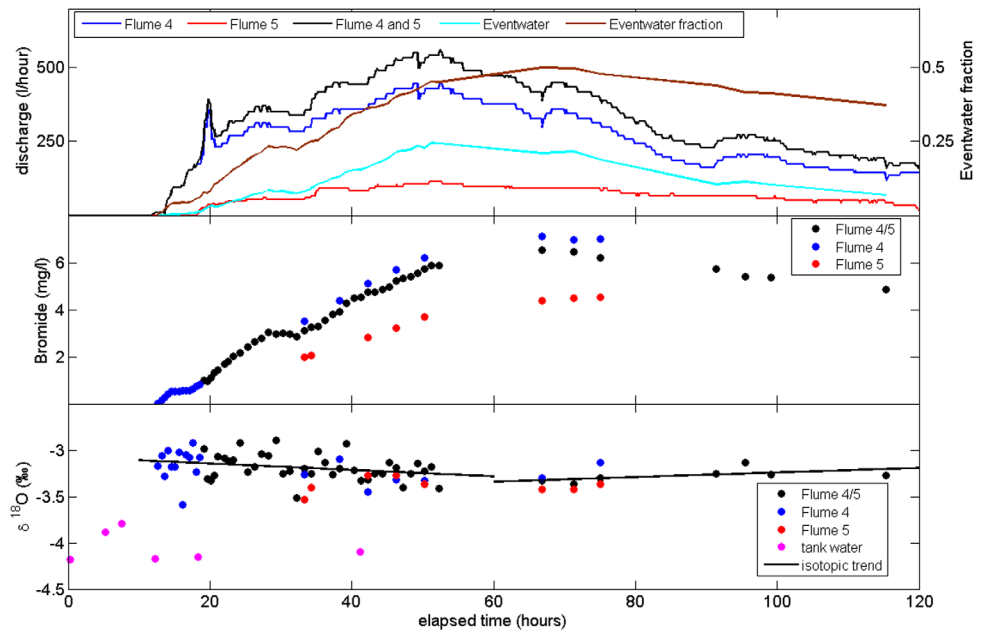


Figure 3. Bromide and O-18 concentrations of water in the trench outflow. New water fraction inferred from bromide concentrations peaked at 50% sixteen h after irrigation ceased, mirroring the time (14:35 h) to peak dye concentrations at the start of the experiment.

values <0.2 mg/L and 5% for values >0.2 mg/L. A Turner 10-AU Fluorometer was used to analyze the trench water samples for dye concentrations. Water samples were analyzed for $\delta^2\text{H}_{\text{H}_2\text{O}}$ and $\delta^{18}\text{O}_{\text{H}_2\text{O}}$ composition using off-axis integrated cavity output laser spectroscopy on a Los Gatos Research Liquid Water Isotope Analyzer (LWIA-24d, Los Gatos Research, Inc.) at Oregon State University. Deuterium values were reported as ratios relative to Vienna Standard Mean Ocean Water (V-SMOW) in standard “delta” notation. Lab standards were routinely verified using isotope ratio mass spectrometry. Analytical precision for $\delta^2\text{H}_{\text{H}_2\text{O}}$ was 1.0‰ and 0.2‰ for $\delta^{18}\text{O}_{\text{H}_2\text{O}}$.

2.9. Calculation of Topsoil and Argillic Hydraulic Conductivities

The average topsoil conductivity was estimated by applying the kinematic wave assumption (hydraulic gradient equal to the slope gradient) to Darcy’s Law and solving for the K value that matched the quasi steady-state trench outflow. To calculate the conductivity of the argillic layer, we assumed the total leakage through the clay was equal to the irrigation input minus the sum of trench flow and Penman-Monteith evapotranspiration during near steady-state conditions at the end of Phase II. We assumed that the pressure head at the bottom of the argillic layer was zero (because the recording piezometer below the argillic did not record saturation), and the thickness of the argillic was 2 m (taken from five measurements in the hill-slope around the plot). Therefore, the hydraulic gradient through the clay was $(h(x) + B_n)/B_n$, where $h(x)$ was the depth of saturation above the Bt horizon at any point x going downslope, and B_n was the normal thickness of the Bt horizon. We calculated the average vertical hydraulic conductivity by iterative solution of the steady-state mass balance equation using the kinematic wave assumption with leakage and with and without downslope unsaturated flow. For the initial guess of the iterative solution, we assumed a linear wedge of saturated thicknesses from zero at the top of the plot to the measured saturated thickness in the row 1 piezometers. The hillslope mass balance is expressed as

$$\text{Net Irrigation} = \text{leakage} + \text{saturated downslope flow} + \text{unsaturated downslope flow} \quad (1)$$

$$Px \cos(\theta) = k_c \int_0^x \left\{ \frac{h(x) + C_n}{C_n} \right\} dx + k_t \tan(\theta) h(x) + \tan(\theta) \int_{-(N-h(x))}^0 k(\varphi) d\varphi \quad (2)$$

where P = irrigation or rainfall rate minus the ET rate, x = distance downslope, k_c , k_t = saturated hydraulic conductivities of the clay and topsoil, respectively, C_n = normal thickness of the clay layer, N = normal

thickness of the topsoil, θ = slope angle, φ = pressure head, and $h(x)$ = normal thickness of saturated layer above impeding layer at point x .

We assumed that head was constant normal to the slope, so pressure heads decreased linearly with normal distance above the perched water table. For downslope unsaturated flow, we used the van Genuchten moisture release curve and conductivity parameters previously fitted to moisture release data for these soils [Du et al., 2016]. Most simplistically, we also calculated the average vertical hydraulic gradient by assuming a uniform unit hydraulic gradient through the Bt horizon whereby equation (2) simplifies to:

$$P_x \cos(\theta) = k_c x + k_r \tan(\theta) h(x) + \tan(\theta) \int_{-(n-h(x))}^0 k(\varphi) d\varphi \quad (3)$$

Pore velocities for the preferential flow networks were calculated from the downslope distances from the dye tracer transects to the trench divided by their time of peak concentration. Conductivities for the preferential flow networks were calculated from the pore velocities again using the kinematic assumption of hydraulic gradient equal to the slope and a porosity of 0.33 (corresponds to a bulk density of 1.78 g cm^{-3}) measured in core samples of the E horizon. National Resources Conservation Service soil surveys also report high bulk densities of $1.6 - 1.75 \text{ g cm}^{-3}$ for the upper layers of the Fuquay soil series translating to porosities of 0.34–0.4.

3. Results

3.1. Time Series of Soil Moisture, Piezometric Behavior, and Trench Flows

Soil moisture in the topsoil (“shallow” sensors) responded after about an hour (14 mm) of irrigation, and then rose very rapidly to levels that stayed constant during the first phase of irrigation (Figure 2c). When the irrigation rate was reduced in Phase II, moisture levels dropped slightly to a new equilibrium level. Soil moisture at the soil-argillic interface (“deep” sensors) did not respond until about 8 h or 100 mm of irrigation, at which time soil moisture at the interface also rose rapidly, reaching an equilibrium level for Phase I irrigation within 2 h. Soil moisture time series were partially dependent on slope position, with much slower recession in the low slope positions following cessation of irrigation (Figure 2c).

Perching of a saturated lens began in the Bt horizon, and water levels rose rapidly within the Bt horizon after saturation was initiated (Figure 2a). Du et al. [2016] observed the same hydrologic behavior of the Bt layer during natural storms. Water level rise in the topsoil was slower, reflecting the differences in soil moisture release curves of the layers [Du et al., 2016]. Saturation was never observed in the recording piezometer below the Bt horizon, indicating unsaturated percolation from the bottom of the clay layer. Saturation in the lower (row 1) piezometers was observed soon after soil moisture in the Bt horizon began rising. The three piezometers in row 1 began responding at 8:45, 10:00, and 12:45 h, or 103, 120, and 136 mm of applied water, respectively (Figure 2b). Flume 4 started flowing at 11:20 h, before the last of the row 1 piezometers responded (Figures 2b and 2d).

Row 2 piezometers responded later and more variably, with responses initiating from 14:45 h (168 mm) up to 36 h (314 mm) (Figure 2b). Row 3 piezometers recorded either no perching or only trace levels of saturation. The uppermost piezometer in the plot, in row 4, responded early, along with the row 1 piezometers, but water levels never rose above 40 mm. Another row 4 piezometer also rose to 40 mm of saturation for a few hours.

Flumes 4 and 5 featured substantially different interflow generation thresholds, 131 and 208 mm, respectively (Figure 2d), even though their contributing areas are adjacent and the surface topography is similar, indicating substantial differences in flow pathways, storages, or percolation rates over relatively small scales. Flume 4 also produced much higher flows through the experiment, cumulatively yielding 80% of outflow. Despite differences in hydrologic behavior between the two flumes, the flume 4 and flume 5 hydrographs were similar in shape (Figures 2 and 3).

One difference in the flume 4 and 5 hydrographs was an apparent pressure wave response that occurred in flume 4 flows within 20 min of restarting the irrigation after the 10 min cessation necessary to switch sprinkler heads during the Phase I to Phase II transition (Figure 2). Flume 5 had only begun flowing less than an hour before the change in irrigation rates, and the flume 5 hydrograph showed no abrupt transitions after

the change. Flume 4 had already been flowing for 7 h and was flowing at a substantial rate when the irrigation recommenced, and water levels in most of the piezometers in rows 1 and 2 had already reached levels near their eventual maxima, so the flow system feeding flume 4 was well-primed. Pressure wave theory and observations predict that the celerity of pressure waves is similar to the pore velocity of water when available storage in the soils is high but the celerity of the pressure wave is much faster than the pore velocity when available soil storage is low [Rasmussen *et al.*, 2000, Waswa *et al.*, 2013]. At flume 4, trench flow spiked 20 min after irrigation recommenced, indicating a pressure wave celerity much faster than observed dye tracer velocities. Piezometer levels were only checked hourly, but two piezometers in row 1 and two more in row 2 also suggested a pressure wave response following recommencement of irrigation. These four piezometers had the highest total heads and were among the five earliest responding piezometers. The data suggested that part of the flow system draining to flume 4 had reached a highly responsive state for which any sudden increase in input caused a pressure pulse to propagate to a part of the discharge region. In this three dimensional flow field, no path length can be ascribed to the apparent pressure wave from the available data, so celerity could not be calculated.

Shortly after the switch to lower Phase II irrigation rates at 18:58 h, piezometer levels, soil moisture, and the trench outflows appeared to reach near steady-state conditions during which piezometer levels increased slowly and erratically from 24 to 36 h after just 245 to 315 mm of irrigation (Figures 2b, 2c, and 3). Cumulative outflows were relatively steady between hour 24 (318 L/h) and hour 33 (337 L/h), peaking in-between at 371 L/hr. After this first quasi steady-state period, Row 1 and 2 piezometer levels and outflows increased until about hour 48 (388 mm), and then appeared to reach another quasi, albeit erratic, steady-state. We ceased irrigation at 51:18 h (407 mm) and used this later period to estimate plot-scale conductivities for the topsoil layer and the argillic Bt horizon (discussed below). All wells and flows began dropping immediately following cessation of irrigation.

After irrigation ceased, piezometers in row 2 drained much faster than those in row 1, indicating that flow was still moving downslope and feeding the lower wells. Eventually most wells in row 1 reached a level at which water levels dropped very slowly, indicating these wells were located in local low spots with relatively tight clay below. The upslope piezometers remained dry during drainage. Trench flow continued for 100 h (4.2 days) following cessation of irrigation. Perching recorded in the piezometers continued from 60 h (2.5 days) to over 130 h (5.4 days) depending on position.

3.2. Conservative Tracer Behavior and Event Water Fractions

Bromide concentrations in the outflow water increased almost linearly throughout the irrigation period, peaked 16 h after the cessation of irrigation, and then dropped steadily during the remainder of the monitored recession period (in the absence of irrigation) (Figure 3). Rising bromide concentrations temporarily leveled off during the latter part of the first quasi-equilibrium period from 24 to 36 h (Figure 3). Bromide concentrations differed consistently and substantially between flumes 4 and 5 (Figure 3). The event water fraction in the trench outflow peaked at 50%. Cumulatively, preevent water comprised 64% of the trench outflow. Over the first 130 h, we recovered 180 g of bromide at the trench, 19% of the approximately 960 grams that were applied.

Small but measurable concentrations of bromide were measured as soon as flow began (Figure 3), indicating some event water moved as bypass flow through preferential pathways, a finding substantiated by the arrival of the surface dyes (below). Dye concentrations reached their peak shortly after the initiation of flow (Figure 4), when the event water fraction was barely above zero.

3.3. Dye Tracer Arrival and Preferential Flow Velocities and Conductivities

Both dye tracers arrived with the wetting front (Figure 4), with concentrations of both tracers peaking at one and 3 h after flow initiated in flume 4 (12:15 and 14:35 h after irrigation began). Steenhuis *et al.* [1994] observed similar dye transport attributed to matrix bypass flow. Although the fluorescein traveled approximately 10 m to the trench, its peak arrival coincided with that of rhodamine that had traveled only 4.5 m to the trench. These arrival times indicate dye tracer velocities in the range of 31–82 mm/h and corresponding conductivities of 864–2240 mm/h (porosity = 0.33, slope = 0.12).

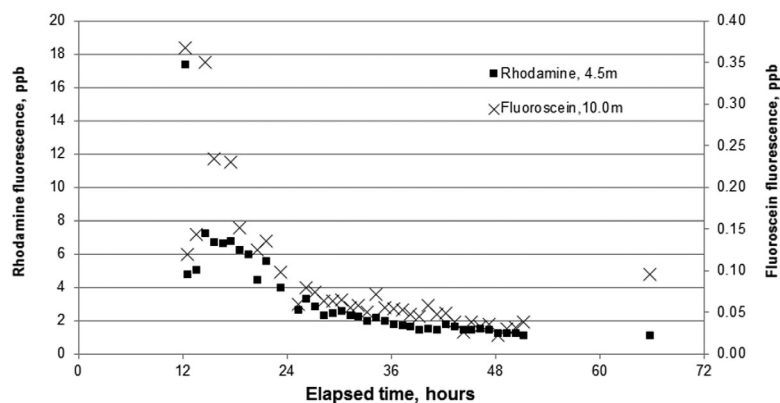


Figure 4. Time series of measured fluorescence of dye tracers fluorescein and rhodamine in the trench outflow. Both dye tracers arrived simultaneously with the wetting front, even though the horizontal travel distance of fluorescein was twice the distance of rhodamine (travel distances listed in the legend). Concentrations of both tracers peaked twice: in the first sample (at 12:15) and again at 14:35 h after irrigation began, indicating dye tracer velocities in the range of 0.31–0.82 m per h. Pore velocities yield K_{sat} values of 864–2240 mm/h (assuming porosity = 0.33, slope = 0.12), 1.6–4.2 times higher than the average topsoil conductivity (460 mm/h) determined from steady-state flow, indicating that the early-arriving dye traveled by pathways with substantially higher conductivities than the bulk value of the topsoils. The simultaneous arrival of the dye tracers indicates that water collected and mixed in a subsurface storage feature near the base of the slope before “spilling” into the trench.

3.4. Longitudinal Piezometric Profiles and Plot-Scale Conductivity Estimates

Because almost all of the upper piezometers (rows 3 and 4) remained dry throughout the experiment, flow from the upper half of the slope may have percolated or moved downslope either as unsaturated flow in the sand or saturated flow within the BE transition (Figure 5). The kinematic wave solution with unsaturated flow (Figure 6) indicates that downslope unsaturated flow could account for the lack of perching observed in the piezometers in rows 3 and 4, as predicted by the modeling of *Zaslavsky and Sinai* [1981]. We observed 10 and 20 cm variations in heads across rows 1 and 2, respectively, indicating hydraulic gradients driving some flow transverse to the plot slope.

During the final quasi steady-state period, the net plot input rate (irrigation rate minus evapotranspiration rate estimated from the Penman-Monteith equation) was 1099 L/h, and trench outflows were 530 L/h, so inferred leakage through the clay was 569 L/h. Assuming a 12 m wide cross section, an average wedge thickness of 0.8 m, and a gradient equal to the slope of 0.12, the bulk saturated conductivity of the topsoil was estimated to be 460 mm/h. Values of the conductivity of the underlying Bt horizon from the four estimation techniques were in close agreement: 2.4, 2.4, 2.5, and 2.9 mm/h for the linear wedge, saturated kinematic steady-state flow with percolation, saturated/unsaturated kinematic steady-state flow with percolation, and the unit hydraulic gradient through the Bt horizon, respectively. At this scale, all estimation techniques for the conductivity of the Bt horizon were in close agreement, but the steady-state solution for saturated and unsaturated kinematic flow best matched the observed piezometer levels (Figure 6), so the value of 2.5 mm/h for the Bt horizon conductivity has the most evidentiary support.

Penman-Monteith estimates of actual evapotranspiration averaged 4.3 mm/d over the irrigation period occurring mostly in the middle of the day when rates exceeded 0.5 mm/h. In Phase II, the irrigation rate was 6 mm/h, so ET significantly damped the midday net input rate.

3.5. Behavior of N and P in Solution

While the event/preevent water fraction increased throughout the irrigation, the behavior of nutrients over the irrigation experiment varied by nutrient type. Overall, mean soluble reactive phosphorus (SRP) and ammonium concentrations in interflow (Figure 7) were much lower (SRP: $< 2 \mu\text{g P/L}$, ammonium: $12 \mu\text{g N/L}$) than the concentrations in tank water (SRP: $33 \mu\text{g P/L}$, ammonium: $1236 \mu\text{g N/L}$). In contrast, nitrate concentrations in interflow (mean = $296 \mu\text{g N/L}$) were about 1/3 of the influent concentration ($902 \mu\text{g N/L}$) (Figure 7). Both ammonium and nitrate concentrations varied over the irrigation experiment, but these temporal changes did not appear to be related to day versus night periods (i.e., nutrient concentrations were not lower during the day when nutrient uptake by vegetation may be greater). Stable isotope of nitrate analysis

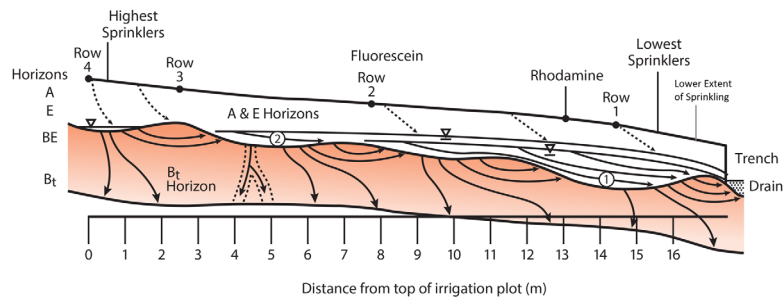


Figure 5. Longitudinal profile of the saturated mound during peak water table conditions during the experiment and inferred flow processes, drawn to scale, for surface slopes of 11–12%. Solid arrows indicate saturated flow, and dashed arrows indicate unsaturated flow. After irrigation ceased, wells in row 2 drained much faster than those in row 1, indicating flow was still moving downslope and feeding the lower wells. Most of the wells in row 1 reached a level at which water levels dropped very slowly, indicating these wells were located in local low spots with relatively tight clay below. Flow from the upper quarter of the slope moved either as unsaturated flow in the sand or within a BE transition horizon and higher conductivity sublayers of the B horizon, or both. The low spot marked 1 is where we assume rhodamine and fluorescein pooled and mixed before spilling simultaneously into the trench. The existence of the low spot marked 2 is inferred from the apparent release of water from an upslope storage area that caused row 1 and 2 piezometer levels and trench outflows to increase after the apparent steady-state situation that lasted from hours 24 to 36. We also inferred that some water must have moved downslope from the Bt horizon to account for the total amount of old water.

showed that $\delta^{18}\text{O}_{\text{NO}_3}$ in trench flow nitrate increased fairly linearly from +5‰ to +20‰ over 60 h, and approached the $\delta^{18}\text{O}_{\text{NO}_3}$ value in tank water of +25‰ (data not shown).

3.6. Cumulative Water Budget Over the Experiment

Over the course of this experiment, 199 mm (equal to 49% of the 407 mm applied water) appeared as interflow in the trench (Figures 8 and 9). Sixty-four percent (128 mm) of the interflow was preevent water. Estimates of preevent water in the topsoils ranged from 62.5 to 100 mm, so preevent water in the topsoil cannot fully account for the total outflow of preevent water even if all tightly held water were stripped from the topsoils and replaced. Some of the interflow must have originated from the Bt and the transitional BE horizon (Figure 5). Visual inspection of the trench face revealed seepage coming from both the BE and Bt horizons (as well as the E horizon above). Penman-Monteith estimates of ET calculated from nearby climate tower data suggest that after 200 h, 8.9% (36.2 mm) had evaporated or transpired, and soil moisture data indicate that only 5.6% (22.7 mm) of event water was still in soil storage in the A, E, and BE horizons at the end of monitoring at 200 h. The residual of 35.9% (148.5 mm) had either leaked past the first meter of the Bt horizon or could not be accounted for.

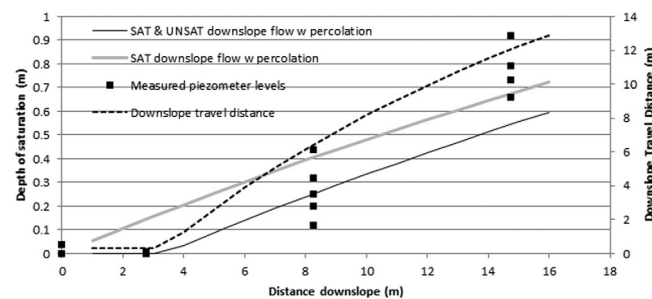


Figure 6. Predictions of water levels (black and grey lines) and downslope travel distances (dotted line) from steady-state kinematic wave equation with percolation in comparison with measured piezometer levels. These distributions of water levels were used to calculate vertical hydraulic gradients along the hillslope length for the estimation of the Bt layer conductivity. The saturated and unsaturated simulation assumes that unsaturated flow above the saturated lens is moving downslope in parallel with the saturated flow whereas the saturated downslope flow simulation assumes vertical unsaturated flow from the soil surface to the saturated zone. Other observations suggest that the lower row of piezometers is sitting in a local low spot, and this may be the cause of the mismatch between measured piezometer levels and predictions from the saturated and unsaturated simulation at this location.

4. Discussion

4.1. Interflow Generation Thresholds and Fill and Spill Behavior

The high interflow generation thresholds of 131 and 208 mm we observed for a relatively dry preevent soil moisture condition bracketed the 160 mm threshold of combined event and preevent water previously modeled with HYDRUS modeling using a free drainage lower boundary condition. These thresholds were much higher than the 60 mm determined from natural storms for which preevent water was not estimated [Du et al., 2016].

The piezometer and flow time series suggest multiple sequential thresholds within the slope and also the

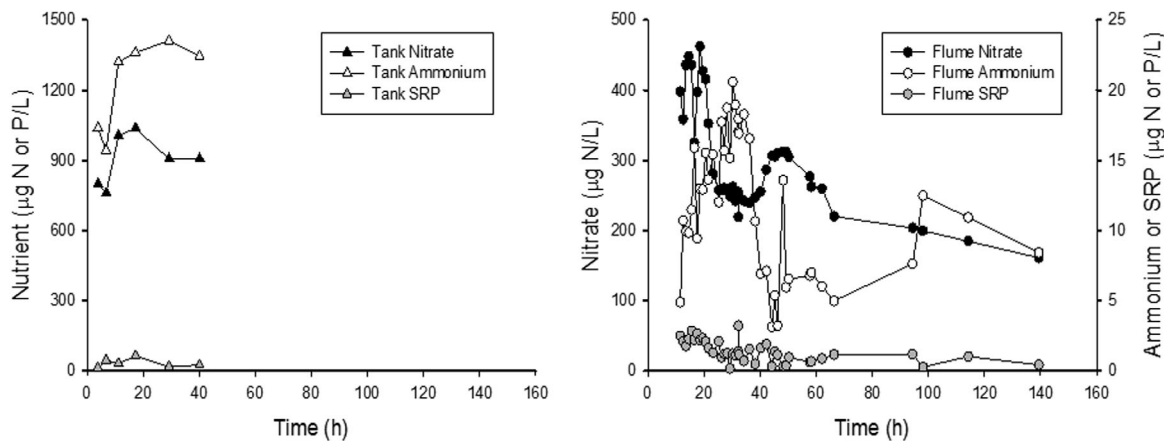


Figure 7. Nitrate, ammonium, and soluble reactive phosphorus (SRP) concentrations in the supply tanks and trench flow water (flow-weighted sample from both flumes) during the irrigation experiment. Mean tank nutrient concentrations were within ranges previously observed in throughfall in Watershed R.

variability of thresholds over relatively short distances. The first threshold observed from the soil moisture time series involved the water necessary for the wetting front to traverse the topsoils and reach the impeding Bt horizon. Then we observed a threshold for bringing the Bt horizon to saturation. Once perching began, we saw evidence of nonsimultaneous fill and spill events that resulted in an apparent stair-stepping of piezometric and flow response. During the quasi steady-state period, piezometer levels in rows 1 and 2 were erratic, possibly as a result of multiple small fill and spill events occurring throughout the lower half of the plot. After the first quasi steady-state period, piezometer levels and outflows both increased steadily again, suggesting that internal hillslope soil storage features somewhere in the mid to upper portion of the plot not measured by our monitoring system had filled and begun to spill downslope (Figure 10). Furthermore, we saw a substantially larger interflow generation threshold for water directed toward flume 5 than for flume 4. Eventually, nearly all of the saturated sections of the soil mantle (except at the top of the irrigation area) apparently connected and near steady-state conditions were achieved (Figure 10).

Several lines of evidence point to concavities in the surface of the Bt horizon as contributing to the storage incorporated in the threshold response. From the simultaneous arrival of dye tracers from the two transects, we infer that there was a low spot in the argillic surface in the vicinity of the row 1 piezometers, and perched water pooled in this low spot until the water level rose high enough to spill downslope into the trench (Figures 5 and 10). During this fill period, the fluorescein and rhodamine mixed in this depression storage feature. When the features spilled downslope, both dyes arrived together. *McGuire and McDonnell* [2010] observed the same phenomenon in a bedrock-controlled hillslope in the Oregon Cascades. Flume 4 began flowing before all row 1 piezometers measured perching, indicating that subsurface flow paths did not follow surface topography directly down the slope, but rather followed low points in the argillic topography. Variation in isotopic signatures between flumes 4 and 5 are indicative of differences in preevent

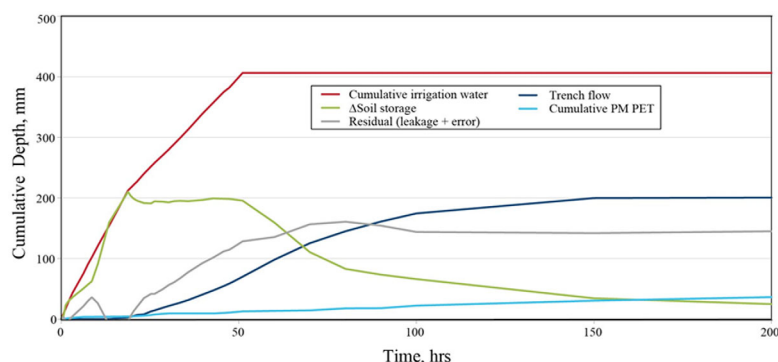


Figure 8. Time series of cumulative input, outputs, soil moisture storage, and residuals of water over the course of the experiment.

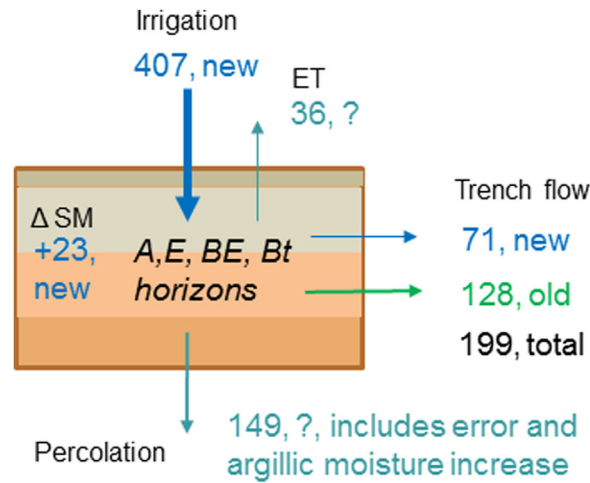


Figure 9. Total inflows, outflows, and net change in soil storage (mm) 200 h after irrigation began, following 149 h of drainage. Blue represents new water fluxes, green represents old water flux, and blue-green with a question mark represents a mix of unknown proportions.

downslope and feeding the lower piezometers. Subsequently, after all piezometers in rows 2–4 had emptied, most piezometers in row 1 reached a level from which water levels dropped very slowly, indicating these piezometers were located in local low spots with relatively tight clay below. Taken together, the very slow late drainage of row 1 piezometers, the simultaneous arrival of the dye tracers, and the underprediction of piezometer levels at this location by the kinematic model all provide evidence for the existence of a low spot in the argillic surface in the vicinity of row 1 (Figures 4 and 5, and 10).

water retention and event water mixing over small spatial scales. The lower flow rates and lower event water fractions in flume 5 suggest that this flume was receiving more water from the B and BE horizons, rather than from the higher conductivity A and E horizons.

These observations are consistent with field [Tromp van Meerveld and McDonnell, 2006] and modeling [Hopp and McDonnell, 2009] evidence of the fill and spill process from the Panola and Maimai sites [Graham and McDonnell, 2010, Graham et al., 2010a] and are consistent with a fill and spill process above and within the argillic layer in this low-relief topography.

After irrigation ceased, piezometers in row 2 drained much faster than those in row 1 (Figure 2b), indicating that flow was still moving

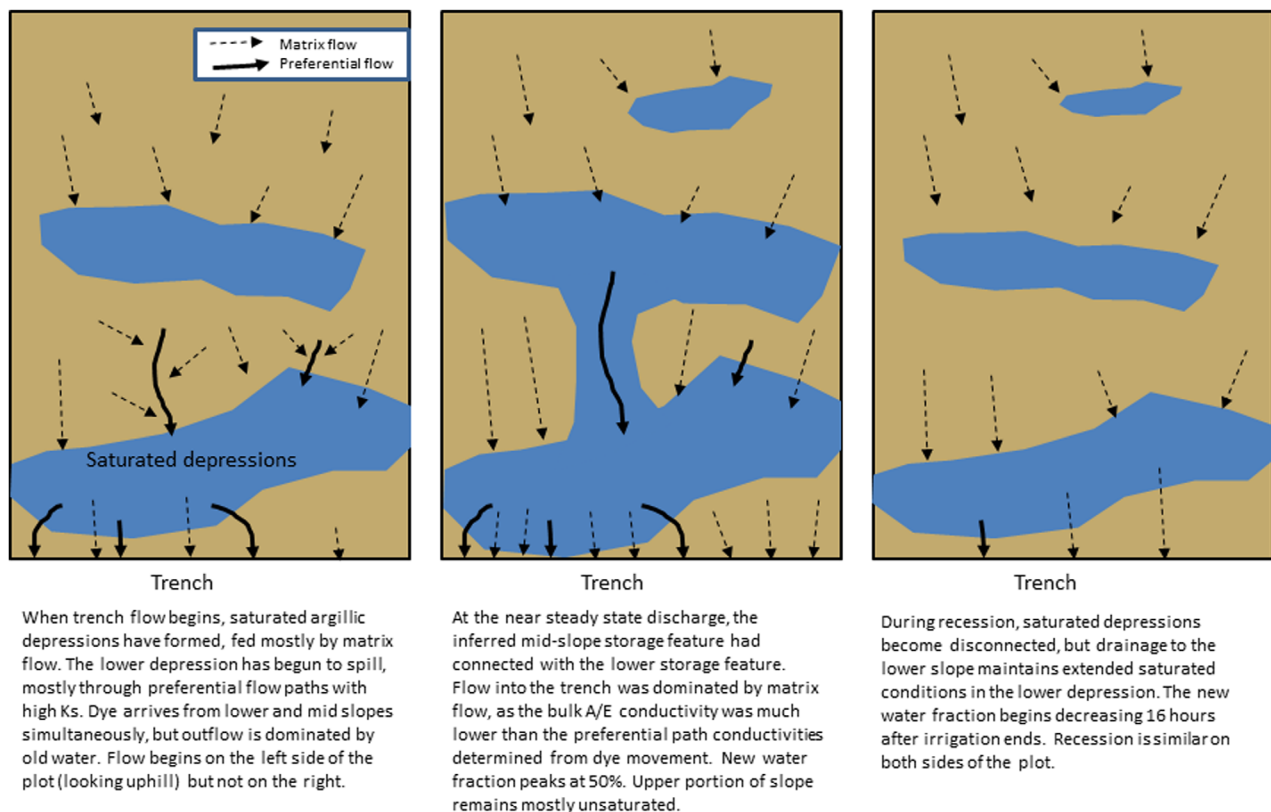


Figure 10. Inferred progression over the irrigation experiment of saturated depressions on the argillic surface as well as matrix and preferential flow.

These observations raise questions about pedogenesis and the nature of subsurface concavities across geomorphic settings. Why do they form? Are such irregularities a consequence of early soil formation or are they formed much later via tree throw and other biologically mediated processes? While work in geomorphology is tackling this question [e.g., Lutz and Griswold, 1939, Schaetzl, 1986, Roering *et al.*, 2010], the hydrological coupling to these processes remains poorly understood. New nondestructive geophysical insights are needed to help us characterize these features and to begin to incorporate them into predictive flow models given their importance here and elsewhere [e.g., Tromp van Meerveld and McDonnell, 2006]. Our observations have implications for groundwater recharge enhancement where recent modeling has shown that fill elements can greatly enhance vertical recharge to groundwater at the hillslope scale [Appels *et al.*, 2015].

Topsoil moisture levels dropped rapidly after irrigation ceased, suggesting that water storage within the BE and Bt horizons, along with the perched water held in the argillic surface depressions, are important reservoirs to maintain forest transpiration.

4.2. Time Series of Event/Preevent Water

In general, bromide concentrations and event water fractions rose steadily and nearly linearly with irrigation input. They temporarily leveled off during the quasi steady-state period, during which time we infer that a large subsurface storage feature in the middle to upper slope was being filled before spilling, thus delaying event water arrival from that part of the slope. The steady decrease in event water that began 16 h after irrigation ceased and continued through the monitored recession suggests that the slower moving water in the BE horizon featured a larger fraction of preevent water.

Event water fractions in rainfall events observed in other studies vary substantially between and during storms (see review in Klaus and McDonnell [2013]), but our continuous application of a conservative tracer demonstrates that a large part of that variability is due to storm size alone: i.e., the greater the depth of the storm, the greater the event water fraction. This experiment raises but does not address the question of whether rainfall or irrigation intensity also affects the event water fraction (something difficult to test during natural events).

The isotopic signature of the trench flow water with respect to the signature of the irrigation water substantiated the bromide results, but the water isotope data were much noisier and far more difficult to interpret (Figure 3). Event/preevent water fractions calculated from only the isotope data would have had wide confidence bands. We are uncertain about the source of noise in the interflow water isotope concentrations.

4.3. Average and Preferential Flow Conductivities

The conductivities estimated from the dye tracer arrivals assume that flow moved in a straight line downslope and that the hydraulic gradient remained constant and equal to the surface slope. Internal storages created by depressions in the impeding pedogenic layer create an ill-posed inverse problem for determining hydraulic conductivities from pore velocities. The transit time used to estimate the pore velocities is a function of both conductivity and detention in subsurface storage features. Furthermore, hydraulic gradients are also affected by these storage features. Essentially this leaves one equation with three unknowns. By ignoring the detention features and assuming a downslope gradient equal to the slope gradient, the downslope hydraulic conductivity of the preferential flow network is underestimated.

Conductivities determined from dye tracer pore velocities were 1.9–4.9 times the average conductivity of the topsoil determined from steady-state flow, indicating that the flow associated with the upper tail of the travel time distribution (through the preferential flow network) comprised only a small fraction of the flow system. Kung *et al.* [2005] noted that soil hydraulic conductivity can be used to estimate water fluxes and even solute transport when matrix flow dominates, but the lumped conductivity becomes inadequate when convective transport through preferential pathways becomes important. Conductivity varies not only spatially, as has been studied extensively [e.g., Binley *et al.*, 1989, Barth *et al.*, 2001], but at every spatial scale the soil features a web of slower and faster pathways. By using probability density functions to account for state-dependent conductivity distributions, solute transport through this web can be modeled [Kung *et al.*, 2006]. Only a certain amount of flow can be accommodated by the preferential flow network so additional water must pass through the less conductive matrix. The large-scale average conductivity we measured from steady-state fluxes integrated the high conductivities of the preferential flow network and the much lower conductivities measured typically with small-scale infiltrometers and permeameters. Therefore the

conductivity estimates based on dye tracer velocities are not representative of the whole flow system as they primarily integrate over the preferential flow paths. However, the dye tracer velocities provide an upper bound for the distribution of conductivities and help explain the apparent paradox of preevent water dominating the early hillslope outflow (see below, and discussion of the Maimai catchment by *McDonnell and Beven* [2014]). They also explain why the first flush of solutes may travel far ahead of a solute plume traveling through the bulk of the matrix. *Hornberger et al.* [1991] observed the same paradox of surface tracers arriving at the beginning of flow while end member mixing suggested inconsequential amounts of event water at the beginning of flow, but they did not have the benefit of a constant addition of a conservative tracer to help explain their dye tracer results. The lag between the cessation of irrigation and the peak bromide concentration nearly mirrored the time (14:35 h) to peak dye concentrations at the start of the experiment. This suggests that the time to drain the preferential flow network was similar to the time necessary to initiate flow through this network.

The plot-scale average conductivity of the surface soils (460 mm/h) was substantially higher than the median of value of 100 mm/h previously measured with a compact constant head permeameter [*Du et al.*, 2016]. This result is in keeping with what others have found – that large-scale conductivities or calibrated conductivities of surface soils are higher than those determined from small-scale measurements with infiltrometers or permeameters [e.g., *Blain and Milly*, 1991; *Grayson et al.*, 1992; *Brooks et al.*, 2004].

Hydrologists usually conceptualize preferential flow as moving through visually apparent macropores, but that was not the case here. No visual macropore flow was observed at the trench face during this experiment or previous natural rainfall events. Nevertheless, dye transport indicated a network of higher conductivity zones and features through which the rapid preferential flow moved.

4.4. Downslope Travel Distances

This hillslope was underlain by a permeable sandy clay loam argillic Bt horizon with a substantial saturated conductivity (2.5 mm/h) relative to low intensity rainfall rates. Nevertheless, the slope featured a strong contrast between the average conductivities of the topsoil (460 mm/h) and that of the impeding layer (2.5 mm/h)—enough to drive interflow when the soil moisture and subsurface detention storage thresholds were exceeded. However, the low slope of this hillslope segment counteracted the high ratio (159) of topsoil to impeding layer conductivities, limiting average downslope travel distances to at most 12 m at the base of this segment (calculated following *Jackson et al.* [2014]). Because of the ensemble of hydraulic conductivity values, there was also a distribution of downslope travel distances, and solutes moving through the preferential flow system (K values in the range of 2000 mm/h) might move nearly 40 m downslope before percolating through the Bt horizon. In either case, interflow on this slope would mostly act to redistribute percolation downslope from the point of infiltration, rather than transport water all the way to the riparian valley (200 m from the irrigated slope). Since the downslope travel distance is a function of the thickness of the perched water table, the water table profile observed in this experiment suggests that flow from only about half the irrigated hillslope would reach the trench (Figures 5 and 6), which roughly matches our observation that the total trench flow was equal to 49% of the total irrigation input.

4.5. Nutrient Cycling and Transport

Cycling processes differed by nutrient (ammonium, nitrate, and phosphorus) over the timescale of this event. Concentrations of ammonium in interflow were much lower than nitrate, despite similar concentrations in the tank water, suggesting greater removal (via sorption or uptake) of ammonium relative to nitrate. Further, low concentrations of soluble reactive phosphorus (SRP) and ammonium in interflow relative to the concentrations in tank water suggest that removal rates of ammonium and SRP were high. The various pathways by which ammonium and phosphorus could be taken up include assimilation, nitrification (for ammonium), and sorption; however, we could not determine which process was most dominant.

Outflow nitrate concentrations varied temporally throughout the experiment, and these dynamics may reflect variation in soil water chemistry across the hillslope and continued mixing as the contributing area of hillslope changed over the experiment (as illustrated in Figure 10). We were not able to measure nutrient concentrations in soil water prior to the irrigation experiment because the sampling piezometers were dry; however, mean nitrate concentration in trench flow for 2 storms in 2011 and 4 storms in 2012 ranged from 40 to 104 $\mu\text{g N/L}$ with a peak concentration across all storms of 190 $\mu\text{g N/L}$ [*Griffiths et al.*, 2016]. These

nitrate concentrations measured prior to the experiment were lower than nitrate measured in the trench outflow during the irrigation experiment (range: 161–462 $\mu\text{g N/L}$; Figure 7) suggesting the nitrate in trench flow reflected the added nitrate (mean concentration in tank = 902 $\mu\text{g N/L}$). $\delta^{18}\text{O}_{\text{NO}_3}$ also corroborated this observation as trench water nitrate increased linearly throughout the irrigation experiment in a similar temporal pattern to that observed for bromide (Figure 3), suggesting nitrate movement along the hillslope was more similar to a conservative tracer. Overall, the irrigation experiment revealed different characteristics in nutrient cycling and transport in a hillslope, and suggests that nitrate is a mobile nutrient [e.g., Bormann *et al.*, 1968; Mitchell *et al.*, 1996].

4.6. Value of the Multitracer Approach: Water and Solute Transit Time Differences

Individually, several of our tracers might have led us to different and somewhat contradictory conclusions. By themselves, the dye tracers would have caused us to overestimate the average conductivity of the topsoil. When coupled with conductivity estimates based on mass balance and Darcy’s law, the dye tracers suggested the existence of preferential flowpaths not associated with visually apparent macropores, and revealed a wide distribution of conductivity values within an apparently homogenous soil mantle (also observed by Kung *et al.* [2005]). The event water fraction determined from the bromide outflows would not have revealed the high end of the hydraulic conductivity range nor the pooling and mixing of event water in argillic depressions. The stable water isotope data helped substantiate the inference from the bromide data, but in isolation would not have provided a clear time series of the event water fraction. The nutrient tracers revealed relatively rapid assimilation, sorption, and uptake processes for ammonium and

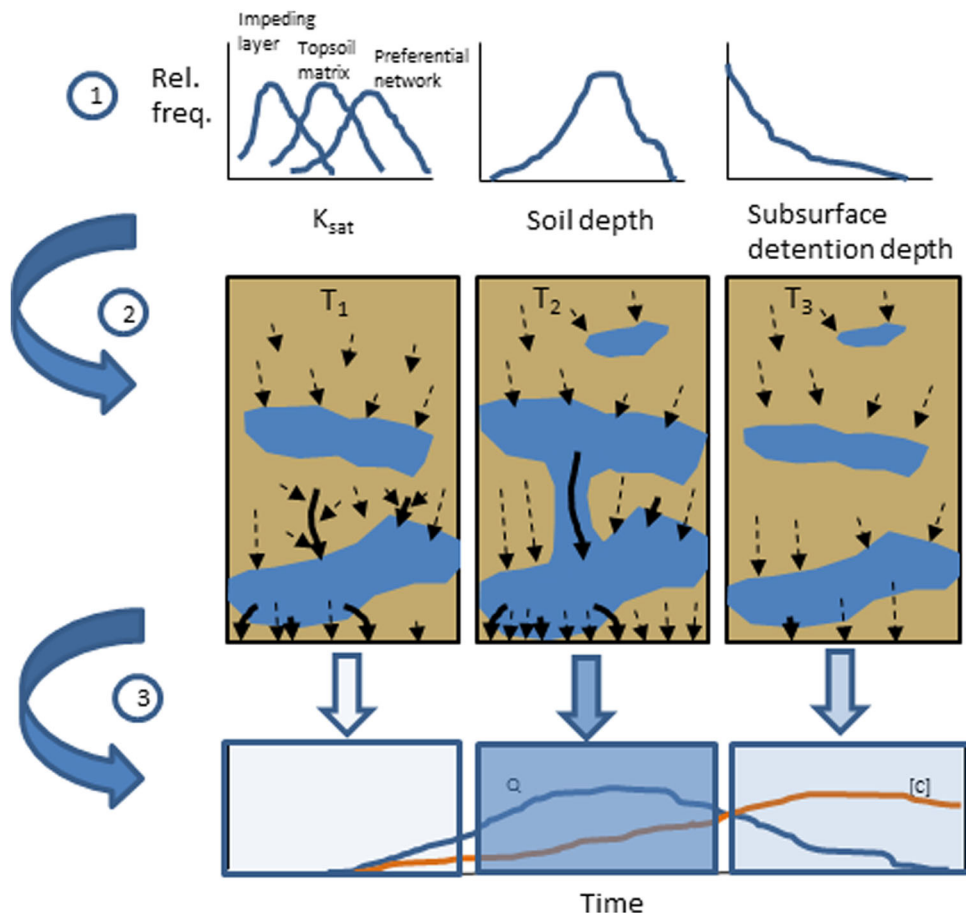


Figure 11. Hillslope exports of water and solutes integrate spatially and temporally varying processes controlled by the interactions of the distributions of conductivities, soil depths, and subsurface detention features. (1) Dominant hillslope controls exist as continuous distributions. (2) Interactions of these distributions across space create semiindependent flow paths with unique interflow thresholds; downslope connectivity that varies with moisture content (cascading thresholds); and spatially variable recharge. (3) The cumulative hillslope flow and solute hydrograph integrates the responses of the ensemble of pathways.

phosphorus that affected outflow chemistry even during a massive precipitation event. In contrast, nitrate transport was much more conservative.

So what does this all mean? Our findings suggest that one's view of hillslope flow processes depends on the scale, number, and frequency of observations of state variables and outputs. Less frequent and/or less numerous observations of fewer tracers would have produced different inferences about hydrologic processes within the slope. Flow and solute transport on this hillslope encompasses a distribution or ensemble of thresholds and flow paths that vary over space (Figure 11). Furthermore, the time series of flows and solute fluxes integrate a number of relatively independent flow paths with variations in their controls and internal storages. These findings suggest re-thinking the standard approach to end member mixing and source apportionment at the catchment outlet [e.g., *Steenhuis et al.*, 1994]. Our field has suffered from interpretations biased by specific techniques. A classic example is the work at the Maimai catchment where consideration of the behavior of multiple tracers (separately and over the many years of study), resulted in many different interpretations of system behavior. Early work by *Mosley* [1979] using dye tracers suggested a macropore-dominated system with rapid movement of event water to streams. However, subsequent isotope-based 2-component mixing revealed outflows dominated by old water [*Pearce et al.*, 1986; *Sklash et al.*, 1986]. Other work at Maimai examining interflow hydrographs across the hillslope illustrated variable and complex responses to storms. *Weiler and McDonnell* [2007] showed how using combined Br and isotope tracers on the same hillslope over many weeks could reconcile event-driven preferential flow mobilization and between-event advective-diffusive flow and transport. Merging and synthesizing these separate lines of enquiry has been challenging but ultimately has yielded a more complete system understanding [*McDonnell*, 1990; *McGlynn et al.*, 2002].

Hillslope controls on flow pathways exist in a continuum, and the relative magnitude and importance of processes depends on the topography and lithology of each slope. This hillslope lies on the opposite end of the spectrum from the steep, bedrock-controlled, and very wet Maimai catchments [see *McGlynn et al.*, 2002], but subsurface flow processes in both are partly controlled by the topography and nature of the subsurface impeding layer and not the surface topography. In both of these contrasting hillslopes, the subsurface flow dynamics and mixing processes are much more complicated than surface topography would suggest.

5. Conclusions

Conductivities determined from dye travel times and bulk conductivities determined from steady-state flows together revealed a distribution of hydraulic conductivities in relatively homogenous loamy sand topsoils that allowed some solute export through bypass flow far in advance of the bulk of the wetting front. Surface-applied dye tracers moved and arrived with the lead outflows, apparently along preferential flowpaths, and concentrations peaked shortly after trench flow initiated. This preferential network was not associated with visually apparent macropores. Conductivities of the toposils calculated from the dye tracer velocities ranged from 864 to 2240 mm/h and were 1.9 to 4.9 times greater than the bulk conductivity (460 mm/h) determined from mass balance at quasi steady-state. The bulk and the maximum conductivities were much greater than the median value of 100 mm/h for surface conductivities previously measured at this site using small-scale permeameters [*Du et al.*, 2016], substantiating previous observations that small-scale conductivity measurements tend to be low-biased [*Brooks et al.*, 2004].

Dye tracer arrivals, soil moisture time series, piezometric behavior, and trench outflows all suggested sequential and spatially variable thresholds for perching and for interflow initiation. Along the same contour, both the amount of precipitation necessary to initiate perching and the rate of drainage were highly variable. Observations were consistent with the fill and spill concept but suggested multiple successive fill and spill events that affected the progression of flows and piezometer levels through the event. The subsurface depression storage on the argillic surface contributed to large and spatially variable interflow generation thresholds of 131 and 208 mm. Even on a small and apparently homogenous hillslope segment, interflow generation thresholds varied by 59% between the two collection drains, raising the question of how interception trench length and segmentation affect inference.

Event water fractions of the trench outflows increased steadily with the irrigation depth, peaking at 50%. The tight relationship between the depth of irrigation and the event water fraction indicates that high

storm-to-storm variability in event water fractions in the same watersheds observed in past studies may be substantially a function of storm size. The cumulative amount of preevent water in trench flow exiting the slope was greater than the estimate of preevent water in the A and E horizons. This suggests that there was exchange of preevent water in the BE and Bt horizons with event water moving to the trench. The lack of perching in most of the piezometers in the upper half of the plot suggests that some flow moved through higher conductivity layers in the BE transition and Bt horizons, below the level of the piezometers, and some flow moved as unsaturated flow through the sand.

Downslope travel distances on this hillslope were limited by the percolation of water through the argillic Bt horizon. The cumulative water balance for this experiment, along with the piezometric behavior, agreed with predictions by the simple downslope travel distance model proposed by Jackson *et al.* [2014] and by the steady-state kinematic wave equation including percolation through the impeding layer. Cumulative trench outflows equaled 49% of input water, suggesting that about half of the plot area contributed interflow that reached the trench. The observed range of conductivities suggests a distribution of interflow travel distances, so some solutes may travel much farther than would be predicted from the average velocities.

The differential behavior of nutrients applied in the irrigation suggests that cycling processes varied by nutrient (ammonium, nitrate, phosphorus) within the timescale of this artificial event. Nitrate moved rapidly downslope compared to ammonium and phosphorus, and was likely less influenced by biological or physical (sorption) processes. Nitrate concentrations and stable isotopes in the outflow suggested that nitrate moved with interflow essentially as a conservative tracer during the event. Overall, ammonium and phosphorus deposited in rainwater may be tightly cycled at the scale of a hillslope, but nitrate in rainwater may travel farther distances downslope and therefore would be the nutrient of greatest water quality concern if it reached stream water. However, interflow travel distances are short in this watershed (12–40 m for this hillslope; described above) [Jackson *et al.*, 2014], suggesting the contributing area of interflow to stream water is small so nitrate will likely not enter stream water via interflow but rather through the groundwater flowpaths that dominate in these low-relief watersheds [Du *et al.*, 2016; Klaus *et al.*, 2015; Griffiths *et al.*, 2016].

The representative elemental volume concept predicts that the variability of average hydraulic conductivities will diminish and reach an asymptote with increasing spatial scales. The resulting average conductivity is useful for modeling hillslope flows, but the full distribution of hydraulic conductivities [Kung *et al.*, 2006] as well as the scale and connectedness of internal storage features (e.g., concavities in the impeding layer surface) are necessary to explain the movement of solutes. We examined a planar hillslope with apparently uniform soil and vegetation characteristics and found unexpected flow and storage complexities over spatial scales of meters, similar to the observations of Bachmair and Weiler [2014].

References

- Ali, G., D. Tetzlaff, J. J. McDonnell, C. Soulsby, S. Carey, H. Laudon, K. J. McGuire, J. Butte, J. Seibert, and J. Shanley (2015), Comparison of threshold hydrologic response across northern catchments, *Hydrol. Processes*, 29, 3575–3591.
- Ali, G. A., A. G. Roy, M. C. Turmel, and F. Courchesne (2010), Source-to-stream connectivity assessment through end-member mixing analysis, *J. Hydrol.*, 392, 119–135.
- Allen, R. G., et al. (2000), Issues, requirements and challenges in selecting and specifying a standardized ET equation, Proceedings of 4th National Irrigation Symposium, pp 201–208, paper presented at 4th National Irrigation Symposium, Am. Soc. of Civ. Eng.
- Anderson, A. E., M. Weiler, Y. Alila, and R. O. Hudson (2009), Subsurface flow velocities in a hillslope with lateral preferential flow, *Water Resour. Res.*, 45, W11407, doi:10.1029/2008WR007121.
- APHA (2005), *Standard Methods for the Examination of Water and Wastewater*, 21st ed., American Public Health Association, Washington, D. C.
- Appels, W. M., J. Freer, C. Graham, and J. J. McDonnell (2015), Factors affecting the spatial pattern of bedrock groundwater recharge at the hillslope scale, *Hydrol. Processes*, 29(21), 4594–4610, doi:10.1002/hyp.10481.
- Bachmair, S., and M. Weiler (2014), Interactions and connectivity between runoff generation processes of different spatial scales, *Hydrol. Processes*, 28, 1916–1930.
- Barnes, R. T., P. A. Raymond, and K. L. Casciotti (2008), Dual isotope analyses indicate efficient processing of atmospheric nitrate by forested watersheds in the northeastern U.S., *Biogeochemistry*, 90, 15–27.
- Barth, G. R., M. C. Hill, T. H. Illangasekare, and H. Rajaram (2001), Predictive modeling of flow and transport in a two-dimensional intermediate-scale, heterogeneous porous medium, *Water Resour. Res.*, 37(10), 2503–2512.
- Binley, A., K. Beven, and J. Elgy (1989), A physically based model of heterogeneous hillslopes 2. Effective hydraulic conductivity, *Water Resour. Res.*, 25(6), 1227–1233.
- Blain, C. A., and P. C. D. Milly (1991), Development and application of a hillslope hydrologic model, *Adv. Water Resour.*, 14(4), 168–174.
- Bormann, F. H., G. E. Likens, D. W. Fisher, and R. S. Price (1968), Nutrient loss accelerated by clear-cutting of a forest ecosystem, *Science*, 159, 882–884.
- Brooks, E. S., J. Boll, and P. A. McDaniel (2004), A hillslope-scale experiment to measure lateral saturated hydraulic conductivity, *Water Resour. Res.*, 40, W04208, doi:10.1029/2003WR002858.

Acknowledgments

Benjamin Morris did much of the work setting up and running the water distribution and irrigation system. The USFS-SRS Fire crew members, particularly Pat Wright, were instrumental in setting up the storage tanks and running the irrigation pump. Ed Olsen and John Blake of the USFS provided substantial logistical support. Benjamin Morris, Tina Garland, Bob Bahn, Lynsey Long, Samantha Marchman, Kristin Kraseski, and Kyle Dalton assisted with data collection and water sampling during the experiment, and Kitty McCracken assisted with nutrient analyses. Our reviewers greatly improved the telling of this story. Funding and support were provided by the Department of Energy-Savannah River Operations Office through the U.S. Forest Service Savannah River under Interagency Agreement DE-AI09-00SR22188 and from the U.S. Department of Energy's Bioenergy Technologies Program to Oak Ridge National Laboratory. Oak Ridge National Laboratory is managed by UT-Battelle, LLC, for the U.S. Department of Energy under contract DE-AC05-00OR22725. Experimental data and the kinematic wave model can be found at www.hydrology.uga.edu or by contacting C.R. Jackson (rjacks@uga.edu). This manuscript has been authored by UT-Battelle, LLC under contract DE-AC05-00OR22725 with the U.S. Department of Energy. The United States Government retains and the publisher, by accepting the article for publication, acknowledges that the United States Government retains a nonexclusive, paid-up, irrevocable, world-wide license to publish or reproduce the published form of this manuscript, or allow others to do so, for United States Government purposes. The Department of Energy will provide public access to these results of federally sponsored research in accordance with the DOE Public Access Plan (<http://energy.gov/downloads/doe-public-access-plan>).

- Buttle, J. M., and D. L. Peters (1997), Inferring hydrological processes in a temperate basin using isotopic and geochemical hydrograph separation: A re-evaluation, *Hydrol. Processes*, *11*, 557–573.
- Carrera, J., E. Vazques-Sune, O. Castillo, and X. Sanchez-Vila (2004), A methodology to compute mixing ratios with uncertain end-members, *Water Resour. Res.*, *40*, W12101, doi:10.1029/2003WR002263.
- Casciotti, K. L., D. M. Sigman, M. Galanter Hastings, J. K. Böhlke, and A. Hilkert (2002), Measurement of the oxygen isotopic composition of nitrate in seawater and freshwater using the denitrifier method, *Anal. Chem.*, *74*, 4905–4912.
- Debieche, T. H., T. A. Bogaard, V. Marc, C. Emblanch, D. M. Krzeminska, and J. P. Malet (2012), Hydrological and hydrochemical processes observed during a large-scale infiltration experiment at the Super-Sauze mudslide (France), *Hydrol. Processes*, *26*, 2157–2170, doi:10.1002/hyp.7843.
- Delsman, J. R., G. H. P. O. Essink, K. J. Beven, and P. J. Stuyfzand (2013), Uncertainty estimation of end-member mixing using generalized likelihood uncertainty estimation (GLUE), applied in a lowland catchment, *Water Resour. Res.*, *49*, 4792–4806, doi:10.1002/wrcr.20341.
- Driscoll, C. T., et al. (2003), Nitrogen pollution in the northeastern United States: Sources, effects, and management options, *BioScience*, *53*, 357–374.
- Du, E., C. R. Jackson, J. J. McDonnell, J. Klaus, N. A. Griffiths, M. F. Williamson, J. L. Greco, and M. Bitew (2016), More fill, less spill: Interflow behavior over a low-angle argillic layer, *J. Hydrol.*, *534*, 648–658.
- Feaster, T. D., J. M. Shelton, and J. C. Robbins (2015), Preliminary peak stage and streamflow data at selected USGS streamgaging stations for the South Carolina flood of 2015, *U.S. Geol. Surv. Open File Rep. 2015-1201*, 19 pp., doi:10.3133/ofr20151201.
- Garel, E., V. Marc, S. Ruy, A. L. Cognard-Plancq, S. Klotz, C. Emblanch, and R. Simler (2012), Large scale rainfall simulation to investigate infiltration processes in a small landslide under dry initial conditions: The Draix hillslope experiment, *Hydrol. Processes*, *26*, 2171–2186.
- Garrett, C. G., V. M. Vulava, T. J. Callahan, and M. L. Jones (2012), Groundwater-surface water interactions in a lowland watershed: Source contribution to stream flow, *Hydrol. Processes*, *26*, 3195–3206.
- Graham, C., and J. J. McDonnell (2010), Hillslope threshold response to storm rainfall: (2) Development and use of a macroscale model, *J. Hydrol.*, *393*(1), 77–93, doi:10.1016/j.jhydrol.2010.03.008.
- Graham, C., J. J. McDonnell, and R. Woods (2010a), Hillslope threshold response to storm rainfall: (1) A field based forensic approach, *J. Hydrol.*, *393*(1):65–76, doi:10.1016/j.jhydrol.2009.12.015.
- Graham, C. B., W. van Verseveld, H. B. Barnard, and J. J. McDonnell (2010b), Estimating the deep seepage component of the hillslope and catchment water balance within a measurement uncertainty framework, *Hydrol. Processes*, *24*, 3631–3647.
- Grayson, R. B., I. D. Moore, and T. A. McMahon (1992), Physically based hydrologic modeling: 2. Is the concept realistic?, *Water Resour. Res.*, *28*(10), 2659–2666.
- Griffiths, N. A., C. R. Jackson, J. J. McDonnell, J. Klaus, E. Du, and M. Bitew (2016), Dual nitrate isotopes clarify the role of biological processing and hydrologic flowpaths on nitrogen cycling in subtropical low-gradient watersheds, *J. Geophys. Res. Biogeosci.*, *121*, 422–437, doi:10.1002/2015JG003189.
- Harpold, A. A., S. W. Lyon, P. A. Troch, and T. S. Steenhuis (2010), The hydrological effects of lateral preferential flow in a glaciated watershed in the northeastern USA, *Vadose Zone J.*, *9*(2), 397–414.
- Hewlett, J. D., and A. R. Hibbert (1963), Moisture and energy relations in a sloping soil mass, *J. Geophys. Res.*, *68*(4), 1081–1087.
- Hopp, L., and J. J. McDonnell (2009), Connectivity at the hillslope scale: Identifying interactions between storm size, bedrock permeability, slope angle and soil depth, *J. Hydrol.*, *376*, 378–391, doi:10.1016/j.jhydrol.2009.07.047.
- Hornberger, G. M., P. G. Germann, and K. J. Beven (1991), Throughflow and solute transport in an isolated sloping soil block in a forested catchment, *J. Hydrol.*, *124*, 81–99.
- Howarth, R. W., et al. (1996), Regional nitrogen budgets and riverine N & P fluxes for the drainages to the North Atlantic Ocean: Natural and human influences, *Biogeochemistry*, *35*, 75–139.
- Jackson, C. R., M. Bitew, and E. Du (2014), When interflow also percolates: Downslope travel distances and hillslope process zones, Invited Commentary, *Hydrol. Processes*, *28*, 3195–3200.
- Kasnavia, T., and D. A. Sabatini (1999), Fluorescent dye and media properties affection sorption and tracer selection, *Groundwater*, *37*(3), 376–381.
- Kilgo, J. C., and J. I. Blake (2005), *Ecology and Management of a Forested Landscape*, 479 pp., Island Press, Washington, D. C.
- Klaus, J., and J. J. McDonnell (2013), Hydrograph separation using stable isotopes: Review and evaluation, *J. Hydrol.*, *505*, 47–64, doi:10.1016/j.jhydrol.2013.09.006.
- Klaus, J., E. Zehe, M. Elsner, C. Külls, and J. J. McDonnell (2013), Macropore flow of old water revisited: Experimental insights from a tile-drained hillslope, *Hydrol. Earth Syst. Sci.*, *17*(1), 103–118.
- Klaus, J., J. J. McDonnell, C. R. Jackson, E. Du, and N. A. Griffiths (2015), Where does streamwater come from in low relief forested watersheds? A dual isotope approach, *Hydrol. Earth Syst. Sci.*, *19*, 125–135.
- Kung, K. J. S., E. J. Kladvko, T. J. Gish, T. S. Steenhuis, G. Bubenzer, and C. S. Helling (2000), Quantifying preferential flow by breakthrough of sequentially applied tracers: Silt loam soil, *Soil Sci. Soc. Am. J.*, *64*, 1296–1304.
- Kung, K. J. S., M. Hanke, C. S. Helling, E. J. Kladvko, T. J. Gish, T. S. Steenhuis, and D. B. Jaynes (2005), Quantifying pore-size spectrum of macropore-type preferential pathways, *Soil Sci. Soc. Am. J.*, *69*, 1196–1208.
- Kung, K. J. S., E. J. Kladvko, C. S. Helling, T. J. Gish, T. S. Steenhuis, and D. B. Jaynes (2006), Quantifying the pore-size spectrum of macropore-type preferential pathways under transient flow, *Vadose Zone J.*, *5*, 978–989.
- Lindberg, S. E., G. M. Lovett, D. D. Richter, and D. W. Johnson (1986), Atmospheric deposition and canopy interactions of major ions in a forest, *Science*, *231*, 141–145.
- Lutz, H. J., and F. S. Griswold (1939), The influence of tree roots on soil morphology, *Am. J. Sci.*, *237*, 389–400.
- McDonnell, J. J. (1990), A rationale for old water discharge through macropores in a steep, humid catchment, *Water Resour. Res.*, *26*(11), 2821–2832.
- McDonnell, J. J., and K. Beven (2014), Debates—The future of hydrological sciences: A (common) path forward? A call to action aimed at understanding velocities, celerities, and residence time distributions of the headwater hydrograph, *Water Resour. Res.*, *50*, 5342–5350, doi:10.1002/2013WR015141.
- McDonnell, J. J., D. D. Brammer, C. Kendall, N. Hjerdt, L. K. Rowe, M. Stewart, and R. A. Woods (1998), Flow pathways on steep forested hillslopes: The tracer, tensiometer, and trough approach, in *Environmental Forest Science*, edited by K. Sassai, pp. 463–474, Kluwer Acad., Boston.
- McGlynn, B. L., J. J. McDonnell, and D. D. Brammer (2002), A review of the evolving perceptual models of hillslope flowpaths at the Maimai catchments, New Zealand, *J. Hydrol.*, *257*, 1–26.
- McGuire, K. J., and J. J. McDonnell (2010), Hydrological connectivity of hillslopes and streams: Characteristic time scales and nonlinearities, *Water Resour. Res.*, *46*, W10543, doi:10.1029/2010WR009341.

- McGuire, K. J., M. Weiler, and J. J. McDonnell (2007), Integrating tracer experiments with modeling to assess runoff processes and water transit times, *Adv. Water Resour.*, *30*, 824–837.
- Mitchell, M. J., C. T. Driscoll, J. S. Kahl, G. E. Likens, P. S. Murdoch, and L. H. Pardo (1996), Climatic control of nitrate loss from forested watersheds in the northeast United States, *Environ. Sci. Technol.*, *30*, 2609–2612.
- Monteith, J. L. (1965), Evaporation and the environment, in the movement of water in living organisms, in *Symposia of the Society for Experimental Biology*, pp. 205–234, Soc. of Exp. Biol., Swansea, Cambridge Univ. Press.
- Mosley, M. P. (1979), Streamflow generation in a forested watershed, New Zealand, *Water Resour. Res.*, *15*(4), 795–806.
- Mulholland, P. J. (1993), Hydrometric and stream chemistry evidence of three storm flowpaths in the Walker Branch Watershed, *J. Hydrol.*, *151*, 291–316.
- Pearce, A. J., M. K. Stewart, and M. G. Sklash (1986), Storm runoff generation in humid headwater catchments 1. Where does the water come from?, *Water Resour. Res.*, *22*(8), 1263–1272.
- Rasmussen, T. C., R. H. Baldwin Jr., J. F. Dowd, and A. G. Williams (2000), Tracer vs. pressure wave velocities through unsaturated saprolite, *Soil Sci. Soc. Am. J.*, *64*(1), 75–85.
- Roering, J. J., J. Marshall, A. M. Booth, M. Mort, and Q. Jin (2010), Evidence for biotic controls on topography and soil production, *Earth Planet. Sci. Lett.*, *298*(1), 183–190.
- Schaetzl, R. J. (1986), Complete soil profile inversion by tree uprooting, *Phys. Geogr.*, *7*(2), 181–189.
- Sebestyen, S. D., E. W. Boyer, J. B. Shanley, C. Kendall, D. H. Doctor, G. R. Aiken, and N. Ohte (2008), Sources, transformations, and hydrological processes that control stream nitrate and dissolved organic matter concentrations during snowmelt in an upland forest, *Water Resour. Res.*, *44*, W12410, doi:10.1029/2008WR006983.
- Shiau, B. J., D. A. Sabatini, and J. H. Harwell (1993), Influence of rhodamine WT properties on sorption and transport in subsurface media, *Groundwater*, *31*(6), 913–920.
- Sigman, D. M., K. L. Casciotti, M. Andreani, C. Barford, M. Galanter, and J. K. Böhlke (2001), A bacterial method for the nitrogen isotopic analysis of nitrate in seawater and freshwater, *Anal. Chem.*, *73*, 4145–4153.
- Sklash, M. G., M. K. Stewart, and A. J. Pearce (1986), Storm runoff generation in humid headwater catchments 2. A case study of hillslope and low-order stream response, *Water Resour. Res.*, *22*(8), 1273–1282.
- Soulsby, C., J. Petry, M. J. Brewer, S. M. Dunn, B. Ott, and I. A. Malcolm (2003), Identifying and assessing uncertainty in hydrological pathways: A novel approach to end member mixing in a Scottish agricultural catchment, *J. Hydrol.*, *274*, 109–128.
- Steenhuis, T. S., J. Boll, G. Shalit, J. S. Selker, and I. A. Merwin (1994), A simple equation for predicting preferential flow solute concentrations, *J. Environ. Qual.*, *23*, 1058–1064.
- Tromp van Meerveld, H. J., and J. J. McDonnell (2006), Threshold relations in subsurface stormflow: 2. The fill and spill response, *Water Resour. Res.*, *42*, W02411, doi:10.1029/2004W003800.
- Tromp van Meerveld, H. J., N. E. Peters, and J. J. McDonnell (2007), Effect of bedrock permeability on subsurface stormflow and the water balance of a trenched hillslope at the Panola Mountain Research Watershed, Georgia, USA, *Hydrol. Processes*, *21*, 750–769.
- Uchida, T., I. Tromp-van Meerveld, and J. J. McDonnell (2005), The role of lateral pipe flow in hillslope runoff response: An intercomparison of non-linear hillslope response, *J. Hydrol.*, *311*(1), 117–133.
- Vitousek, P. M., J. D. Aber, R. W. Howarth, G. E. Likens, P. A. Matson, D. W. Schindler, W. H. Schlesinger, and D. G. Tilman (1997), Human alterations of the global nitrogen cycle: Sources and consequences, *Ecol. Appl.*, *7*, 737–750.
- Waswa, G. W., A. D. Clulow, C. Freese, P. A. L. Le Roux, and S. A. Lorentz (2013), Transient pressure waves in the vadose zone and the rapid water table response, *Vadose Zone J.*, *12*(1), doi:10.2136/vzj2012.0054.
- Weiler, M., and J. J. McDonnell (2007), Conceptualizing lateral preferential flow and flow networks and simulating the effects on gauged and ungauged hillslopes, *Water Resour. Res.*, *43*, W03403, doi:10.1029/2006WR004867.
- Zaslavsky, D., and G. Sinai (1981), Surface hydrology: Causes of lateral flow, *Hydrol. Div. ASCE*, *107*, 37–52.